

Pulsating active matter

Yiwei Zhang and Étienne Fodor

Department of Physics and Materials Science, University of Luxembourg, L-1511 Luxembourg, Luxembourg

In active matter, interacting units convert fuel into sustained dynamics. When activity drives individual motion, particles undergo self-propulsion. It yields nonequilibrium states, such as collective directed motion, observed in many living and synthetic systems. In dense regimes where crowding hinders motion, collective states still emerge, such as contraction waves in living tissues, even when directed motion merely plays any role. Inspired by cell dynamics in tissues, undergoing mechanical deformation with only negligible displacement, we assume here that activity drives individual pulsation through periodic change in size. The competition between repulsion and synchronisation triggers an instability which promotes various dynamical patterns. We study the mechanisms underlying the emergence of patterns, and characterize the corresponding transitions. We also compare our patterns with those of reaction-diffusion, and rationalize this analogy from a hydrodynamic perspective. Overall, our results reveal that, in dense environments, pulsation of synchronised particles is a generic route to contraction waves.

Active matter features injection of energy at individual level to sustain nonequilibrium dynamics [1, 2]. The interplay between particle interaction and individual activity opens the door to collectives without any equilibrium equivalent. In many studies, activity takes the form of self-propulsion: Each particle converts the energy provided by some fuel into motion. Depending on microscopic symmetries, self-propelled particles can exhibit flocking transition [3, 4] and/or motility-induced phase separation [5, 6], for instance. In dense regimes, self-propulsion shifts the glass transition [7]. It also controls the solid-fluid transition in assemblies of cells whose area and perimeter vary with interactions [8, 9].

Activity is not restricted to self-propulsion in general. In biological tissues, living cells use chemical energy to undergo mechanical deformation. For instance, collectively increasing and decreasing their size in a periodic and synchronised fashion [10]. To maintain constant packing fraction, local increase in density yields nearby decrease: Tissues must accommodate coexistence between contracting and expanding regions. This promotes propagation of contraction waves and pulses, as reported both in vivo [11–13] and in vitro [10, 14–19]. Some models, from particles [16, 20] to hydrodynamics [21, 22], capture these waves regarding activity as a combination of self-propulsion and contraction.

The emergence of collective contraction is of tremendous importance in many biological contexts. During morphogenesis, mechanochemical coupling yields wave propagation driving the early stages of embryonic development [23–25]. In cardiac tissue, electromechanical coupling leads to contraction pulses spontaneously organizing in patterns [26–28], some of which signal arrhythmogenesis [29, 30]. In uterine tissue, a similar coupling regulates large-scale contraction during labor [31, 32]. For all cases, understanding how to control contractile patterns is a first step toward mitigating various health disorders.

It is hardly credible that driving individual motion should be the dominant nonequilibrium factor when cells

barely move. Even when biological tissues behave as solids, collectives supported by individual deformation can still emerge. The challenge is then to identify the key ingredients generically yielding such collectives. To this end, inspired by recent works [33–37], we formulate a model of pulsating particles where activity only sustains size oscillations. We delineate conditions where contraction waves indeed emerge, promoting a plethora of dynamical patterns. Importantly, we reveal an analogy with reaction-diffusion [38, 39], which helps rationalize the rich phenomenology of pulsating active matter.

We consider the overdamped dynamics of N deforming particles in two dimensions, interacting via pair-wise repulsion U and synchronisation \mathcal{T} , in terms of their positions $\{\mathbf{r}_i\}$ and phases $\{\theta_i\}$. U and \mathcal{T} are short ranged, with θ_i setting the interaction range

$$\sigma(\theta_i) = \sigma_0 \frac{1 + \lambda \sin \theta_i}{1 + \lambda}, \quad (1)$$

where σ_0 is the largest radius value, and $\lambda < 1$ controls the amplitude of radius fluctuation (Fig. 1). All particles are subject to the same drive ω , which sustains their periodic deformation through phase oscillations:

$$\begin{aligned} \dot{\mathbf{r}}_i &= -\mu \sum_j \partial_{\mathbf{r}_i} U(a_{ij}) + \sqrt{2D} \boldsymbol{\xi}_i, & a_{ij} &= \frac{|\mathbf{r}_i - \mathbf{r}_j|}{\sigma(\theta_i) + \sigma(\theta_j)}, \\ \dot{\theta}_i &= \omega - \sum_j \left[\mathcal{T}(a_{ij}, \theta_i - \theta_j) + \mu_\theta \partial_{\theta_i} U(a_{ij}) \right] + \sqrt{2D_\theta} \eta_i, \end{aligned} \quad (2)$$

where $\{\mu, \mu_\theta\}$ and $\{D, D_\theta\}$ are respectively the mobilities and diffusion coefficients of positions and phases, and $\{\boldsymbol{\xi}_i, \eta_i\}$ are uncorrelated, isotropic Gaussian white noises with zero mean. We take $U(a) = U_0(a^{-12} - 2a^{-6})$ and $\mathcal{T}(a, \theta) = \varepsilon \sin(\theta)$ for $a < 1$, where U_0 and ε determine the strengths of repulsion and synchronisation, respectively; $U(a) = 0 = \mathcal{T}(a, \theta)$ otherwise. Repulsion minimizes particle overlap, which promotes a homogeneous density profile, and impedes (facilitates) the expansion (contraction) of particles whenever they are in contact.

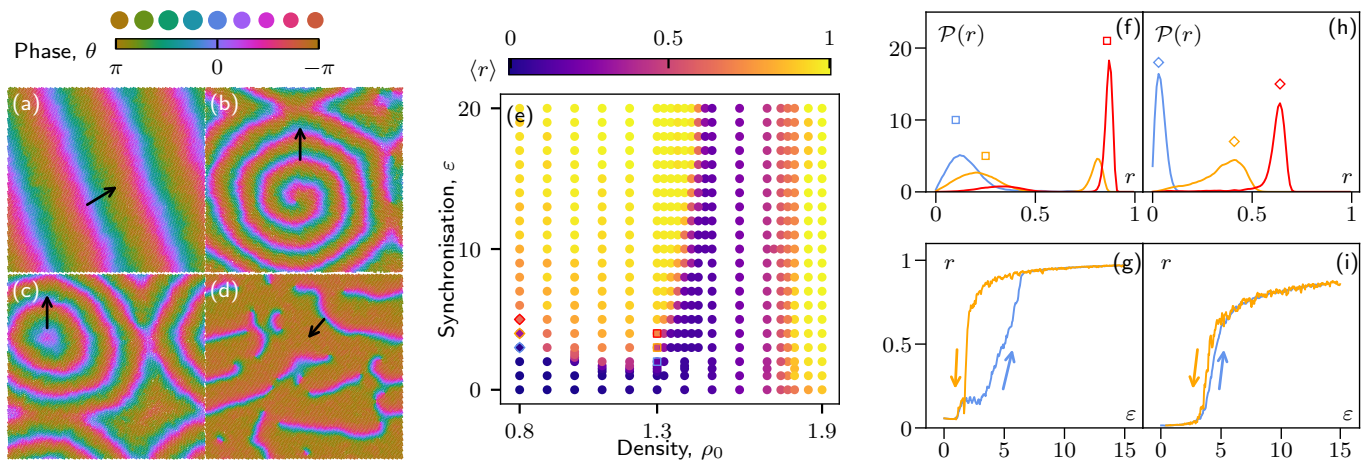


FIG. 1. Contraction waves propagate along black arrows: (a) planar, (b) spiral, (c) circular, and (d) turbulent waves [40]. (e) The phase diagram distinguishes order at high $\langle r \rangle$, where all particles have the same size, from disorder at low $\langle r \rangle$. Order comes with size cycling at moderate ρ_0 , and it is arrested at large ρ_0 . Disorder has a uniform profile at small ρ_0 , whereas it accommodates inhomogeneities at higher ρ_0 , yielding contraction waves at sufficiently high ε . (f-g) At $\rho_0 = 1.3$ (squares in (e)), the transition is discontinuous with metastability. The distribution of r varies between unimodal and bimodal, and hysteresis appears when increasing (decreasing) ε in blue (orange). (h-i) At $\rho_0 = 0.8$ (diamonds in (e)), the transition seems continuous without metastability. The distribution of r stays unimodal, and hysteresis is reduced.

Synchronisation puts a cost at any phase difference between neighbours, thus favoring a uniform phase profile.

In contrast with previous works on deforming particles [33, 34], the packing fraction $\varphi = \pi \sum_i (\sigma(\theta_i)/L)^2$ here varies in time when particles are cycling. Above a given density, repulsion precludes that all particles simultaneously reach their largest size. The competition between repulsion and synchronisation can then destabilize the uniform phase profile, eventually yielding the emergence of contraction waves (Figs. 1(a-d)). In what follows, we analyze the transitions towards wave formation, we identify the corresponding microscopic mechanisms, we obtain a hydrodynamic description of the system, and we examine its analogies with reaction-diffusion dynamics. Overall, our results reveal that, despite the absence of any reaction, driving periodic mechanical deformations of densely packed particles is a route to collectives bearing similarities to reaction-diffusion.

The uniform profile is a fully synchronized state, with most particles having constantly the same size, whereas contraction waves accommodate particles with various phases. In that respect, we regard the emergence of waves as a transition from order to disorder in terms of the synchronisation parameter

$$r = \frac{1}{N} \left| \sum_{j=1}^N e^{i\theta_j} \right|. \quad (3)$$

We detect such a transition by varying the total density ρ_0 and the synchronisation strength ε , which control the repulsion-synchronisation trade-off. Interestingly, we delineate three transitions in terms of the averaged parameter $\langle r \rangle$ (Fig. 1(e)): (i) at high density ($\rho_0 > 1.6$),

the transition merely depends on ε , (ii) at small density ($\rho_0 < \rho_c$, $\rho_c \approx 1.3$), the phase boundary has ε decreasing with ρ_0 , and (iii) at moderate density ($\rho_c < \rho_0 < 1.5$), it has ε increasing with ρ_0 . Although they share the same signature in $\langle r \rangle$, we now demonstrate that they are distinct order-disorder transitions.

At small density, particles can vary their size with only moderate overlap. The ordered and disordered states respectively correspond here to particles all cycling in phase, and particles cycling with phase differences. The effect of repulsion in phase dynamics is subdominant compared with synchronisation. Completely neglecting the former, our setting is akin to the seminal Kuramoto model [41], albeit neighbour identity now varies in time. Given that all phases are driven at the same frequency, the ordered state stabilizes whenever the synchronisation overcomes the noise. At mean-field level, this requires $\rho_0 \varepsilon$ greater than a factor proportional to D_θ , which qualitatively reproduces the behavior of the corresponding phase boundary ($d\varepsilon/d\rho_0 < 0$).

At high density, the system is too jammed for particles to cycle their phase. The ordered state is here arrested, with particle sizes fluctuating around an average value given by close packing, without any phase current. We decompose repulsion as $\partial_{\theta_i} U = (\partial_\varphi U)(\partial_{\theta_i} \varphi)$, with $\partial_\varphi U$ independent of $\{\theta_i\}$ to first approximation: $(\partial_\varphi U) \varphi(\{\theta_i\})$ plays the role of an external potential constraining phase fluctuations. The drive tilts this potential as $(\partial_\varphi U) \varphi(\{\theta_i\}) - \omega \sum_i \theta_i$. At small ω (equivalently, large $\partial_\varphi U$), phases are trapped in a local minimum of the tilted potential, yielding dynamical arrest. In this regime, the potential contribution is overwhelm-

ingly dominant compared with synchronisation, so that the phase boundary is independent of ε .

Reducing ρ_0 decreases $\partial_\varphi U$. Fluctuations then trigger jumps between local minima of the tilted potential, which promotes transient cycling of size. At large ε , local cycling propagates between nearest neighbours, yielding contraction waves moving in an arrested background (Fig. 1(d)). Such waves destabilize the ordered state, yielding disorder *with* dynamical patterns, distinct from the disordered state at small ε and small ρ_0 . Interestingly, spatial coexistence between arrested and cycling particles leads to form pairs of defects connected by bands of particles with equal phase. Such pairs spontaneously form, move, and annihilate (see movie in [40]), in analogy with defect turbulence in reaction-diffusion systems [42]. As ρ_0 gets smaller, more particles are prone to cycling, which increases the wave size, and reduces the proportion of arrested particles. Deep in the disordered state, all particles are cycling, and waves spontaneously organize into specific structures: Either planar, spiral, or circular waves (Figs. 1(a-c)). Correspondingly, defects are now more stable, and their number is much reduced. Eventually, further decreasing ρ_0 , the system enters the cycling ordered state.

In short, waves emerge at large ε and moderate ρ_0 as a transition destabilizing either the cycling or the arrested ordered state, respectively from small and large ρ_0 . The latter clearly stems from the coexistence between arrested and cycling particles. To rationalize the former, we examine how the distribution $\mathcal{P}(r)$ varies through the transition (Fig. 1(f)). Starting from the disordered state, where \mathcal{P} is peaked at small r , \mathcal{P} becomes bimodal as the system enters the ordered state, with weight shifting from small to large r . This indicates the existence of a metastable regime where both states are linearly stable. Such a scenario is robust all along the phase boundary $d\varepsilon/d\rho_0 > 0$. Starting deep in the ordered state and reducing ε , a fluctuation eventually destabilizes the global synchronisation and triggers a discontinuous transition towards small r (Fig. 1(g)). Conversely, starting from the disordered state and reducing ε reveals hysteresis, another signature of metastability. A similar analysis of the transition at small ρ_0 shows that \mathcal{P} now stays unimodal (Fig. 1(h)), the increase/decrease of r with ε appears continuous, and the hysteresis is weak (Fig. 1(i)): Metastability progressively disappears when reducing ρ_0 . Indeed, while repulsion is subdominant in the transition at small ρ_0 (for order and disorder without patterns), it drastically changes the character of the transition at higher ρ_0 (where disorder entails patterns).

Repulsion puts a strong constraint on phase dynamics whenever the packing fraction of large particles $\rho_0\pi\sigma_0^2$ is comparable with the close packing value. In this regime, overlap between particles accelerates (decelerates) their contraction (expansion). Therefore, the packing fraction φ oscillates in quadrature with the scaled instantaneous

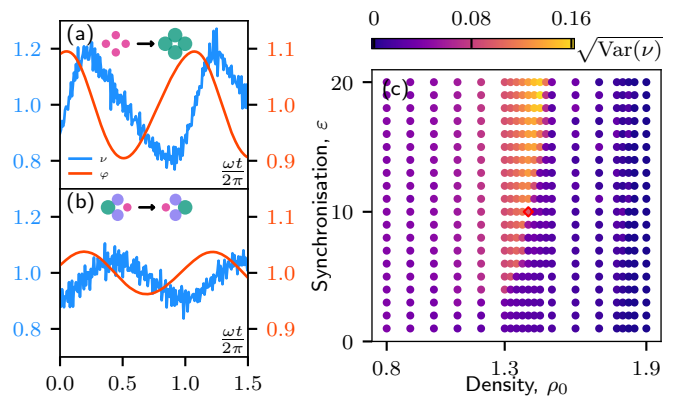


FIG. 2. (a-b) Packing fraction φ and current ν oscillate in quadrature, since particles contract (expand) faster (slower) when they overlap. The oscillation amplitude is higher for globally synchronized particles than for waves (both realizations have the same parameters, diamond in (c)) due to significant overlap at large size. (c) The current variance $\text{Var}(\nu)$ captures the boundary of the order-disorder transition at moderate ρ_0 , see Fig. 1(e) [40].

phase velocity (Figs. 2(a-b))

$$\nu = \frac{1}{N\omega} \sum_{j=1}^N \dot{\theta}_j. \quad (4)$$

In the cycling ordered state, ν decreases faster than it increases due to repulsion, yielding asymmetric oscillations with high amplitude. In the disordered state with patterns, phase shift between neighbours enables a reduced overlap, and oscillations appear sinusoidal with a reduced amplitude. This suggests that the amplitude of oscillations, quantifying the strength of overlap, is actually sufficient to distinguish these states. We detect the corresponding transition in terms of the current variance $\text{Var}(\nu) = \langle \nu^2 \rangle - \langle \nu \rangle^2$ (Fig. 2(c)). In the ordered state, $\text{Var}(\nu)$ increases steadily with ρ_0 until it abruptly drops. The location of this drop is in line with the boundary $d\varepsilon/d\rho_0 > 0$ of the order-disorder transition (Fig. 1(e)).

The averaged parameter $\langle \nu \rangle$ is close to 1 throughout the phase diagram, except in the arrested ordered state where ν vanishes [40]. In that respect, contraction waves can be regarded as the collective strategy which, by introducing local phase shifts, enables to maintain high $\langle \nu \rangle$ even at high ρ_0 . Importantly, synchronisation mitigates high phase shift, promoting bands with equal phase. Therefore, in contrast with previous works [33, 34], synchronisation here stands out as the essential ingredient for stabilizing patterns. In short, the transition at $d\varepsilon/d\rho_0 > 0$ arises from a competition favoring either synchronisation at the cost of overlap, or smaller overlap at the cost of reduced synchronisation.

Our model of pulsating particles, although minimal, already captures the emergence of contraction waves, which propagate throughout the system with only neg-

ligible particle displacement. This is reminiscent of the chemical waves in reaction-diffusion dynamics [38, 39]. Although the microscopics of these dynamics are quite different from ours, it is tempting to draw analogies between the hydrodynamics of pulsating active matter and of reaction-diffusion. For simplicity, setting $\mu = 0$, we neglect the role of repulsion in density fluctuations. In the phase dynamics, we reduce the interaction range as perfectly local: $\sum_j \mathcal{T}(a_{ij}, \theta_i - \theta_j) \approx \pi \sigma_0^2 \varepsilon \sum_j \sin(\theta_i - \theta_j) \delta(\mathbf{r}_i - \mathbf{r}_j)$, and we treat repulsion as $\sum_j \partial_{\theta_j} U(a_{ij}) \approx \pi \sigma_0^2 (\partial_{\varphi} U) \sum_j (\partial_{\theta_j} \varphi) \delta(\mathbf{r}_i - \mathbf{r}_j)$, where $\partial_{\varphi} U$ is again assumed constant. From coarse-graining procedures [40], we obtain a closed dynamics for the local order parameter $A(\mathbf{r}, t) = \sum_j e^{i\theta_j} \delta(\mathbf{r} - \mathbf{r}_j(t))$ to leading order in powers of A and its gradients:

$$\begin{aligned} \partial_t A = & \left(\frac{\bar{\varepsilon} \rho_0}{2} - D_{\theta} + i\omega + D\nabla^2 \right) A - \frac{\bar{\varepsilon}^2 A |A|^2}{4(2D_{\theta} - i\omega)} \\ & - icA \left[\text{Re}(A) + \frac{\bar{\varepsilon} \lambda}{4} \text{Im} \left(\frac{A^2}{2D_{\theta} - i\omega} \right) \right] + \sqrt{\rho_0 D_{\theta}} \Lambda, \end{aligned} \quad (5)$$

where $\bar{\varepsilon} = \pi \sigma_0^2 \varepsilon$, and $c = \mu_{\theta} \lambda (\pi \sigma_0 \sigma(0)/L)^2 (\partial_{\varphi} U)$. The field Λ is a Gaussian white noise with zero mean. This hydrodynamics is analogous to the complex Ginzburg-Landau equation describing a large class of reaction-diffusion systems [43]. The term proportional to c here breaks the gauge invariance $A \rightarrow A e^{i\Phi}$ for any arbitrary Φ . It reveals how the microscopic coupling between repulsion and deformation, respectively contributing to c through $\partial_{\varphi} U$ and λ , affects the gauge symmetry of the hydrodynamic phase.

In the noiseless dynamics, the homogeneous profile is always linearly stable. It can correspond to order $|A| > 0$ or disorder $|A| = 0$. The former can be either arrested or cycling, respectively for constant and time-dependent ψ , where $A = |A|e^{i\psi}$. We obtain analytically the phase boundaries between these states (Fig. 3(a)). The order-disorder transition follows $\bar{\varepsilon} \rho_0 = 2D_{\theta}$, in line with mean-field arguments for the particle-based dynamics. There is no arrest when $c = 0$. The corresponding term, stemming from microscopic repulsion, indeed controls the existence of stationary solutions for ψ . At high density, repulsion gets rapidly enhanced with ρ_0 , so we take $c \propto \rho_0^n$ for $n > 0$. The arrested state then arises at large ρ_0 , and cycling occurs for intermediate density regimes between disordered and arrested states, as expected. In short, our hydrodynamics qualitatively reproduces all the phase boundaries for the homogeneous states observed in microscopics (Fig. 1(e)).

Owing to non-linearities, homogeneous profiles are not the only stable solutions. In the presence of noise, at intermediate ρ_0 and high ε , the hydrodynamics now systematically reaches a non-homogeneous steady state (Figs. 3(b-c)). Such a regime appears between the cycling and arrested states, in qualitative agreement with the emergence of disorder with patterns in microscopics.

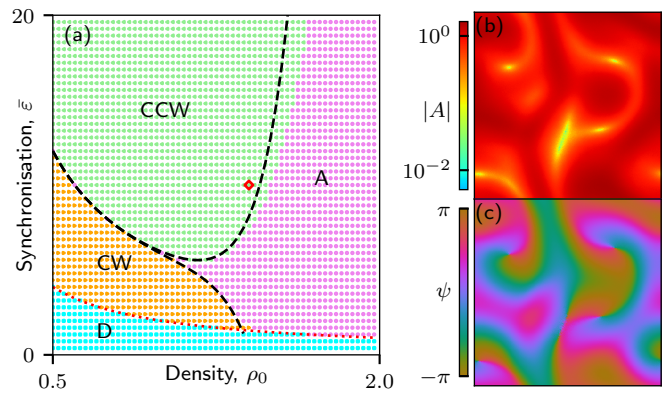


FIG. 3. (a) Phase diagram of homogeneous states in noiseless hydrodynamics: (D) disorder, (A) arrest, (CW) clockwise, and (CCW) counter-clockwise cycles. The red dotted line delineates order-disorder transition. The black dashed lines approximate the stability of arrest [40]. (b-c) In the presence of noise, steady states with motile defects appear instead of homogeneous cycling (diamond in (a)).

In hydrodynamics, it is always associated with motile defects constantly forming and merging, reminiscent of defect turbulence (Fig. 1(d)). Interestingly, we do not observe any wave with stable defects as in microscopics. This suggests that density fluctuations, neglected in our hydrodynamics, play an important role in stabilizing such structures. Indeed, density waves actually propagate along with contraction of particles when defects are stable (Figs. 1(b-c)). It is tempting to speculate that the crossover from motile to stable defects is controlled by the emergence of such waves.

It is striking that our model entails hydrodynamic patterns akin to reaction-diffusion. Indeed, our microscopic dynamics does not feature any reaction, and particle diffusion is strongly hampered in dense regimes of interest. As an insightful analogy, individual pulsation can still be regarded as a chemical reaction, whose coordinate is the particle phase, with ω effectively driving cycles between isomers. Importantly, this drive is a monomolecular reaction. Consistently, hydrodynamic non-linearities all stem from particle interactions: Setting $\bar{\varepsilon} = 0 = c$ reduces to linear dynamics for A . The interplay between synchronisation, repulsion and deformation is then akin to mechano-chemical coupling, which indeed regulates cell size in tissues [44, 45].

Overall, our results show that cells do not need to self-propel to promote contractile patterns. This scenario should be robust when considering more complex interactions. Indeed, if the reference area and perimeter of deforming cells [8, 9] are pulsating, oscillations between elongated and rounded cells is again a route to wave propagation, given local synchronisation of cycling. Interestingly, our model reveals how density controls the crossover between wave types. In cardiac tissues, the emergence of spiral waves and turbulence signals fibrilla-

tion. Various strategies have been proposed to mitigate this while avoiding drastic measures [29, 46, 47]. To this end, our model stands out as the appropriate platform in search of protocols inhibiting specific waves with local perturbation. Moreover, even for dense systems of macroscopic pulsating units, such as human crowds [48], it should still be relevant to delineate strategies which avoid disastrous contraction waves.

We acknowledge insightful discussions with Michael E. Cates, Luke K. Davis, Massimiliano Esposito, Robert L. Jack, David T. Limmer, Alessandro Manacorda, Xia-Qing Shi, Benjamin D. Simons, Thomas Speck, and Julien Tailleur. Work funded by the Luxembourg National Research Fund (FNR), grant reference 14389168.

-
- [1] M. C. Marchetti, J. F. Joanny, S. Ramaswamy, T. B. Liverpool, J. Prost, M. Rao, and R. A. Simha, Hydrodynamics of soft active matter, *Rev. Mod. Phys.* **85**, 1143 (2013).
- [2] C. Bechinger, R. Di Leonardo, H. Löwen, C. Reichhardt, G. Volpe, and G. Volpe, Active particles in complex and crowded environments, *Rev. Mod. Phys.* **88**, 045006 (2016).
- [3] T. Vicsek, A. Czirók, E. Ben-Jacob, I. Cohen, and O. Shochet, Novel type of phase transition in a system of self-driven particles, *Phys. Rev. Lett.* **75**, 1226 (1995).
- [4] H. Chaté, Dry aligning dilute active matter, *Annu. Rev. Condens. Matter Phys.* **11**, 189 (2020).
- [5] Y. Fily and M. C. Marchetti, Athermal phase separation of self-propelled particles with no alignment, *Phys. Rev. Lett.* **108**, 235702 (2012).
- [6] M. E. Cates and J. Tailleur, Motility-induced phase separation, *Annu. Rev. Condens. Matter Phys.* **6**, 219 (2015).
- [7] L. Berthier, E. Flenner, and G. Szamel, Glassy dynamics in dense systems of active particles, *J. Chem. Phys.* **150**, 200901 (2019).
- [8] D. Bi, J. H. Lopez, J. M. Schwarz, and M. L. Manning, A density-independent rigidity transition in biological tissues, *Nat. Phys.* **11**, 1074 (2015).
- [9] D. Bi, X. Yang, M. C. Marchetti, and M. L. Manning, Motility-driven glass and jamming transitions in biological tissues, *Phys. Rev. X* **6**, 021011 (2016).
- [10] S. Zehnder, M. Suaris, M. Bellaire, and T. Angelini, Cell volume fluctuations in mdck monolayers, *Biophys. J.* **108**, 247 (2015).
- [11] A. C. Martin, M. Kaschube, and E. F. Wieschaus, Pulsed contractions of an actin – myosin network drive apical constriction, *Nature* **457**, 495 (2009).
- [12] J. Solon, A. Kaya-Copur, J. Colombelli, and D. Brunner, Pulsed Forces Timed by a Ratchet-like Mechanism Drive Directed Tissue Movement during Dorsal Closure, *Cell* **137**, 1331 (2009).
- [13] S. Armon, M. S. Bull, A. Aranda-Diaz, and M. Prakash, Ultrafast epithelial contractions provide insights into contraction speed limits and tissue integrity, *Proc. Natl. Acad. Sci. U.S.A.* **115**, E10333 (2018).
- [14] X. Serra-picamal, V. Conte, R. Vincent, E. Anon, D. T. Tambe, E. Bazellieres, J. P. Butler, J. J. Fredberg, and X. Trepast, Mechanical waves during tissue expansion, *Nat. Phys.* **8**, 628 (2012).
- [15] T. Sham, G. Estelle, L. Brigitte, C. Olivier, L. Benoît, D.-A. Hélène, and G. François, Collective cell migration without proliferation: density determines cell velocity and wave velocity, *R. Soc. Open Sci.* **5**, 172421 (2018).
- [16] V. Petrolli, M. Le Goff, M. Tadrous, K. Martens, C. Allier, O. Mandula, L. Hervé, S. Henkes, R. Sknepnek, T. Boudou, G. Cappello, and M. Bolland, Confinement-induced transition between wavelike collective cell migration modes, *Phys. Rev. Lett.* **122**, 168101 (2019).
- [17] G. Peyret, R. Mueller, J. d’Alessandro, S. Begnaud, P. Marcq, R.-M. Mège, J. M. Yeomans, A. Doostmohammadi, and B. Ladoux, Sustained oscillations of epithelial cell sheets, *Biophys. J.* **117**, 464 (2019).
- [18] N. Hino, L. Rossetti, A. Marín-Llauradó, K. Aoki, X. Trepast, M. Matsuda, and T. Hirashima, Erk-mediated mechanochemical waves direct collective cell polarization, *Dev. Cell* **53**, 646 (2020).
- [19] D. Boockook, N. Hino, N. Ruzickova, T. Hirashima, and E. Hannezo, Theory of mechanochemical patterning and optimal migration in cell monolayers, *Nat. Phys.* **17**, 267 (2021).
- [20] S. Armon, M. S. Bull, A. Moriel, H. Aharoni, and M. Prakash, Modeling epithelial tissues as active-elastic sheets reproduce contraction pulses and predict rip resistance, *Commun. Phys.* **4**, 216 (2021).
- [21] K. Dierkes, A. Sumi, J. Solon, and G. Salbreux, Spontaneous oscillations of elastic contractile materials with turnover, *Phys. Rev. Lett.* **113**, 148102 (2014).
- [22] S. Banerjee, K. J. C. Utuje, and M. C. Marchetti, Propagating stress waves during epithelial expansion, *Phys. Rev. Lett.* **114**, 228101 (2015).
- [23] C.-P. Heisenberg and Y. Bellaïche, Forces in tissue morphogenesis and patterning, *Cell* **153**, 948 (2013).
- [24] A. Bailles, C. Collinet, J.-M. Philippe, E. M. Pierre-François Lenne, and T. Lecuit, Genetic induction and mechanochemical propagation of a morphogenetic wave, *Nature* **572**, 467 (2019).
- [25] A. Bailles, E. W. Gehrels, and T. Lecuit, Mechanochemical principles of spatial and temporal patterns in cells and tissues, *Annu. Rev. Cell Dev. Biol.* **38**, null (2022).
- [26] A. Karma, Spiral breakup in model equations of action potential propagation in cardiac tissue, *Phys. Rev. Lett.* **71**, 1103 (1993).
- [27] J. Christoph, M. Chebbok, C. Richter, J. Schröder-Schetelig, P. Bittihn, S. Stein, I. Uzelac, F. H. Fenton, G. Hasenfuß, R. F. G. Jr., and S. Luther, Electromechanical vortex filaments during cardiac fibrillation, *Nature* **555**, 667 (2018).
- [28] A. Molavi Tabrizi, A. Mesgarnejad, M. Bazzi, S. Luther, J. Christoph, and A. Karma, Spatiotemporal organization of electromechanical phase singularities during high-frequency cardiac arrhythmias, *Phys. Rev. X* **12**, 021052 (2022).
- [29] A. Karma, Physics of cardiac arrhythmogenesis, *Annu. Rev. Condens. Matter Phys.* **4**, 313 (2013).
- [30] W.-J. Rappel, The physics of heart rhythm disorders, *Phys. Rep.* **978**, 1 (2022).
- [31] J. Xu, S. N. Menon, R. Singh, N. B. Garnier, S. Sinha, and A. Pumir, The role of cellular coupling in the spontaneous generation of electrical activity in uterine tissue, *PLOS ONE* **10**, e0118443 (2015).
- [32] K. M. Myers and D. Elad, Biomechanics of the human

- uterus, *WIREs Syst. Biol. Med.* **9**, e1388 (2017).
- [33] E. Tjhung and T. Kawasaki, Excitation of vibrational soft modes in disordered systems using active oscillation, *Soft Matter* **13**, 111 (2017).
- [34] E. Tjhung and L. Berthier, Discontinuous fluidization transition in time-correlated assemblies of actively deforming particles, *Phys. Rev. E* **96**, 050601 (2017).
- [35] Y. Togashi, Modeling of nanomachine/micromachine crowds: Interplay between the internal state and surroundings, *J. Phys. Chem. B* **123**, 1481 (2019).
- [36] Y. Koyano, H. Kitahata, and A. S. Mikhailov, Diffusion in crowded colloids of particles cyclically changing their shapes, *EPL* **128**, 40003 (2019).
- [37] N. Oyama, T. Kawasaki, H. Mizuno, and A. Ikeda, Glassy dynamics of a model of bacterial cytoplasm with metabolic activities, *Phys. Rev. Research* **1**, 032038 (2019).
- [38] A. M. Turing, The chemical basis of morphogenesis, *Philos. Trans. R. Soc. B Biol. Sci.* **237**, 37 (1952).
- [39] S. Kondo and T. Miura, Reaction-diffusion model as a framework for understanding biological pattern formation, *Science* **329**, 1616 (2010).
- [40] See Supplemental Material at [URL will be inserted by publisher] for details on analytical derivations and numerical simulations, which includes Refs. [49, 50].
- [41] J. A. Acebrón, L. L. Bonilla, C. J. Pérez Vicente, F. Ritort, and R. Spigler, The kuramoto model: A simple paradigm for synchronization phenomena, *Rev. Mod. Phys.* **77**, 137 (2005).
- [42] Q. Ouyang and J.-M. Flesselles, Transition from spirals to defect turbulence driven by a convective instability, *Nature* **379**, 143 (1996).
- [43] I. S. Aranson and L. Kramer, The world of the complex ginzburg-landau equation, *Rev. Mod. Phys.* **74**, 99 (2002).
- [44] J. Howard, S. W. Grill, and J. S. Bois, Turing's next steps: the mechanochemical basis of morphogenesis, *Nat. Rev. Mol. Cell. Biol.* **12**, 392 (2011).
- [45] P. Recho, A. Hallou, and E. Hannezo, Theory of mechanochemical patterning in biphasic biological tissues, *Proc. Natl. Acad. Sci. U.S.A.* **116**, 5344 (2019).
- [46] S. Luther, F. H. Fenton, B. G. Kornreich, A. Squires, P. Bittihn, D. Hornung, M. Zabel, J. Flanders, A. Gladuli, L. Campoy, E. M. Cherry, G. Luther, G. Hasenfuss, V. I. Krinsky, A. Pumir, R. F. G. Jr, and E. Bodenschatz, Low-energy control of electrical turbulence in the heart, *Nature* **475**, 235 (2011).
- [47] N. DeTal, A. Kaboudian, and F. H. Fenton, Terminating spiral waves with a single designed stimulus: Teleportation as the mechanism for defibrillation, *Proc. Natl. Acad. Sci. U.S.A.* **119**, e2117568119 (2022).
- [48] N. Bain and D. Bartolo, Dynamic response and hydrodynamics of polarized crowds, *Science* **363**, 46 (2019).
- [49] D. S. Dean, Langevin equation for the density of a system of interacting Langevin processes, *J. Phys. A: Math. Gen.* **29**, 24 (1996).
- [50] L. B. Cai, H. Chaté, Y. Q. Ma, and X. Q. Shi, Dynamical subclasses of dry active nematics, *Phys. Rev. E* **99**, 10601 (2019).